Cellulose (2018) 25:7261–7275
https://doi.org/10.1007/s10570-018-2052-4

ORIGINAL PAPER

Diallyl dimethyl ammonium chloride-grafted cellulose filter membrane via ATRP for selective removal of anionic dye

Shengchang Lu · Zuwu Tang · Wenyan Li · Xinhua Ouyang · Shilin Cao · Lihui Chen · Liulian Huang · Hui Wu · Yonghao Ni

Received: 7 July 2018 / Accepted: 24 September 2018 / Published online: 28 September 2018

Abstract In this paper, poly(diallyl dimethyl ammonium chloride) (PDADMAC)-grated cellulose filter membranes (cellulose-*g*-PDADMAC) were fabricated via atom transfer radical polymerization (ATRP) for selective removal of anionic dye from wastewater. Gel permeation chromatography (GPC), X-ray photoelectron spectroscopy (XPS), and Fourier transform infrared spectroscopy (FTIR) showed that PDADMAC was grafted onto the filter membrane surface via a controllable living polymerization. The resultant cellulose-*g*-PDADMAC membranes exhibit selective removal for anionic methyl orange (MO) through rapid and facile filtration using model MO/rhodamine B (RB) mixture, due to the electrostatic interaction between quaternary ammonium groups of membrane and the sulfonic groups of MO. The decolorization ratio of MO remains higher than 95% when the graft ratio is 13.3% even after 6 cycles. Cellulose-*g*-PDADMAC also shows effective antimicrobial activities against *S. aureus* and *E. coli*. The modified filter membranes are promising for the potential application in wastewater purification.

Graphical abstract PDADMAC-grated cellulose filter membranes with good recyclability and high antimicrobial activity were fabricated via atom transfer radical polymerization for selective removal of anionic dye from wastewater.

Electronic supplementary material The online version of this article (https://doi.org/10.1007/s10570-018-2052-4) contains supplementary material, which is available to authorized users.

S. Lu · Z. Tang · W. Li · X. Ouyang · S. Cao · L. Chen (✉) · L. Huang · H. Wu (✉) · Y. Ni
College of Material Engineering, Fujian Agriculture and Forestry University, No. 63, Xiyuangong Road, Minhou District, Fuzhou 350108, Fujian, People's Republic of China
e-mail: fafuclh@163.com

H. Wu
e-mail: wuhui@fafu.edu.cn

Y. Ni
Department of Chemical Engineering, Limerick Pulp and Paper Centre, University of New Brunswick, Fredericton, NB E3B 5A3, Canada

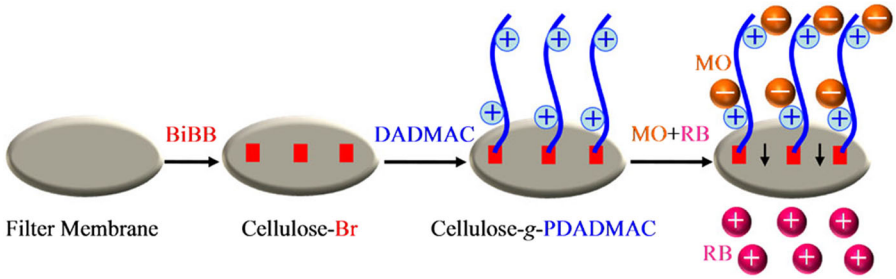

Keywords ATRP · Filter membrane · DADMAC · Dye · Selective removal

Introduction

Textile industries produce large amounts of wastewater which causes great harm to the ecological environment. The main organic pollutants discharged into wastewater are dyes, which are visible and undesirable even at low concentrations in aqueous solution (Crini 2006; Pendergast and Hoek 2011). Most organic dyes create serious threats to human health and aquatic organisms because of their toxicity, non-degradability, teratogenicity, mutagenicity and carcinogenicity (Mathieu-Denoncourt et al. 2014; Mittal et al. 2007). For example, MO is an azo/acid/anionic dye widely used in the textile, paper and printing industries as well as in food and pharmaceutical fields. It can enter the intestinal system inadvertently and even lead to intestinal cancer in humans. Thus, it is crucial to remove dyes from wastewater and process effluents effectively for environmental protection.

Dye wastewater treatments mainly focus on the physical, chemical, biological, acoustical, radiation, and electrical processes (Gupta and Suhas 2009). Among the methods for dye removal from wastewater, membrane filtration is a simple, facile and effective approach (Pendergast and Hoek 2011; Yao et al. 2016). Various highly efficient polymer-based membranes, such as polyethersulfone (PES)/polyethyleneimine nanofibrous membrane (Min et al. 2012), electrospinning poly(ether amine) nanofiber membrane (Fu et al. 2014), polydopamine-coated electrospun polyvinylalcohol/polyacrylicacid membrane (Yan et al. 2015), and metal–organic framework (MOF)/polyethyleneimine hybrid membrane (Yang et al. 2017a) have been extensively applied in dye removal. However, there is still a great challenge to explore low cost and environmentally friendly membrane for removal of dyes.

Cellulose is the most abundant natural polymer across the globe and is low cost, biodegradable, eco-friendly, and highly stable (Habibi 2014; Wang et al. 2016). Although cellulose can adsorb dyes directly, the adsorption capability of natural cellulose is fairly low. However, the unique structure of cellulose makes it available for further modification to improve the adsorption capacity (Hokkanen et al. 2016). Recently, by modifying with specific functional groups such as amino, carboxyl, sulfo group, and magnetic nanoparticles, various materials with well-defined structures and novel properties were reported (Chen et al. 2018; Edgar 2007; Fu et al. 2017; Lin et al. 2016a, b; Qiao et al. 2015; Ran et al. 2014; Tang et al. 2017; Tian and He 2016; Würfel et al. 2018; Wen et al. 2017; Wu et al. 2018; Yang et al. 2017b; Zhang et al. 2017; Zhou et al. 2016). Specifically, functional cellulose-based filtration membranes were fabricated for the treatment of dye wastewater. Cellulose nanocrystals (CNCs)/PES enhanced membranes were constructed by introducing CNCs into a polymeric membrane matrix. The denser skin-layer of the CNC mixed membrane showed compacted nanocomposite structure with smaller surface pore size for higher dye removal (Daraei et al. 2017). Meldrum's acid-modified cellulose nanofiber-based PVDF microfiltration membranes were prepared via solvent-free techniques to remove crystal violet (CV) dyes from water. Owing to the high electrostatic attraction between the positively charged CV dyes and carboxylate groups on the surface of modified cellulose nanofiber, the membrane exhibited better adsorption behavior than the PVDF electrospun membrane (Gopakumar et al. 2017). Palladium

nanoparticles (Pd NPs)-decorated wood membrane was fabricated for efficient wastewater treatment. Due to the unique channel structure of the wood and the catalyst nanoparticles with uniform distribution, the mesoporous Pd NPs/wood membrane had high efficiency for the removal of methylene blue (MB) (Zhang et al. 2017). A MOF membrane was fabricated through the growth of MOF nanoparticles on the surface of a carboxymethylated filter membrane, which can be used for dye separation such as MO/MB mixture solution (Park and Oh 2017). However, most of those reported materials exhibit lack of regeneration, low adsorption capability, or poor antimicrobial activities (Pendergast and Hoek 2011). Moreover, the removal of all the compounds is not always necessary and some valuable chemicals require being recycled (Cheng et al. 2015; Dragan and Dinu 2018). It is desirable to fabricate functional cellulose-based membranes which are capable of selective removal of dyes with recyclability and antimicrobial activities for the practical applications.

Cellulose fibers/products are usually anionic. Their application in the removal of anionic pollutants, such as anionic dyes in waste water from the textile processing, would not be practical, due to charge repulsion. In contrast, if cationic moieties could be grafted onto cellulose macromolecules, new cellulose products could be developed, targeting the removal of anionic dyes in waste water from the textile industry, which is a huge sector in China. PDADMAC with functional quaternized ammonium is cost-effective and commercially-relevant, and it was our choice in this study for rendering cellulose membrane cationic. Herein, cellulose-*g*-PDADMAC membranes via ATRP for the selective separation of anionic dye from the complex dye systems using MO and RB as model pollutants were demonstrated. The resultant cellulose-*g*-PDADMAC showed high cationic density and high stability, due to covalent bonds between cellulose and PDADMAC, and exhibited high selectivity and good recyclability to remove anionic dye molecules, as well as effective antimicrobial activities.

Experiments

Materials

Quantitative filter papers with diameter of 7 cm and average pore size of 1–3 μm were purchased from Hangzhou Special paper Co., Ltd, China. *N*,*N*,*N*′,*N*″,*N*″-pentamethyldiethylenetriamine (PMDETA, 99%), and 2-bromisobutyryl bromide (BiBB, 98%) were obtained from Tokyo Chemical Industry. Copper(I) bromide (CuBr, > 99%) was purchased from Adamas and purified by successive washing with acetic acid and ethanol, and dried under vacuum. MO and RB were purchased from Sigma-Aldrich. DADMAC (60 wt% in water), pyridine, dichloromethane (CH_2Cl_2, 99.9%), acetone, ethanol, and sodium chloride (NaCl) were supplied by Shanghai Aladdin Reagent Co., Ltd, China. Methanolic HCl (0.5 M) was purchased from Acros. All chemicals were analytical grade and used as received. Cellulose ester dialysis tubing (MWCO 500) was purchased from Solarbio S&T CO., Ltd. Peptone, yeast powder, agar, phosphate buffer saline (PBS), *Escherichia coli* (*E. coli*, ATCC 25922) and *Staphylococcus* (*S. aureus*, ATCC 6538) were obtained from Shanghai Luwei Technology Co., Ltd. Ultrapure water (18.2 MΩ cm) obtained by a water purifier (Sichuan Water Purifier Co. Ltd., China) was used for all experiments.

Grafting DADMAC onto the surface of cellulose filter membrane

The schematic for modification of a cellulose filter membrane is shown in Fig. 1. The filter papers were cut into pieces with diameters of 3 cm. To remove the impurities, the membrane was ultrasonicated in CH_2Cl_2 and methanol for 15 min prior to use, respectively. Then the filter membrane was immersed in a solution containing BiBB (0.5 mL, 4.04 mmol), pyridine (0.33 mL, 4.04 mmol) and CH_2Cl_2 (15 mL) under ice-water bath. The mixture was stirred at 0 °C for 15 min and then at room temperature for 24 h. The initiator-functionalized cellulose filter membrane (cellulose-Br) was obtained by washing thoroughly with ethanol and ultrapure water to remove residual reactants, and drying under vacuum at 50 °C for 24 h.

To graft DADMAC onto the surface of filter membrane, the cellulose-Br was immersed into ultrapure water (10 mL) containing PMDETA (31.1 μL,

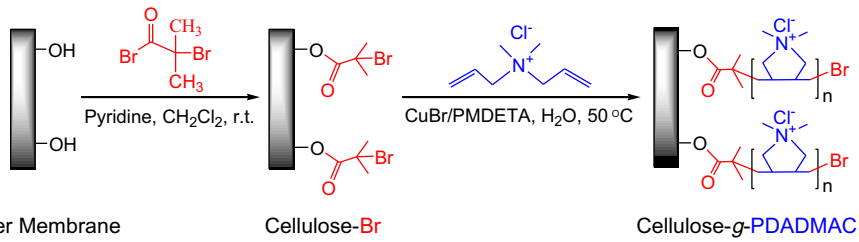

Fig. 1 Schematic of the surface modification on cellulose filter membrane

0.15 mmol). 1.22 or 2.44 mL of DADMAC were added. After the mixture was degassed with two freeze-vacuum-thaw cycles, CuBr (21.6 mg, 0.15 mmol) was added. The system was degassed with another three freeze-vacuum-thaw cycles. Thereafter, the reaction was kept at 50 °C for different time intervals to give the PDADMAC-modified filter membrane (cellulose-*g*-PDADMAC) with various graft ratios. The final cellulose-*g*-PDADMAC filter membranes were obtained by washing thoroughly with acetone and ultrapure water.

Graft ratio was calculated according to the following equation (Sui et al. 2008):

$$\text{Graft ratio} = \frac{W_2 - W_1}{W_1} \times 100\% \quad (1)$$

where W_1 (g) is the oven-dried weight of cellulose-Br, W_2 (g) is the oven-dried weight of cellulose-*g*-PDADMAC.

Cleavage of PDADMAC grafts from cellulose-*g*-PDADMAC membrane

To investigate the number-average molecular weight (M_n) and polydispersity (M_w/M_n) of PDADMAC grafts on cellulose membrane surface, 0.5 g of cellulose-*g*-PDADMAC samples were cut into pieces and hydrolyzed in 15 mL of methanolic HCl overnight under ambient temperature to cleave covalently bound PDADMAC from the cellulose-*g*-PDADMAC. The solution containing cleaved PDADMAC was collected and dialyzed against deionized water for 48 h. Purified PDADMAC solutions were freeze-dried for gel permeation chromatography (GPC) measurements (Zoppe et al. 2016).

Characterization

The M_n and polydispersity of PDADMAC were measured by E2695 GPC (Waters) equipped with differential refractive index detector (RID-20A) and gel column (TSK GMPWxl). The calibration was made with poly(ethylene oxide) (PEO) standards and the eluent was 0.1 N sodium nitrate with a flow rate of 1 mL/min.

The pristine membrane, cellulose-Br and cellulose-*g*-DADMAC were analyzed using X-ray photoelectron spectroscopy (XPS, Thermo Scientific ESCALAB 250Xi), with a standard Al K_α X-ray source (1486.8 eV). The X-ray beam was operated at a current of 10 mA and an acceleration voltage of 15 kV. For wide scan spectra, an energy range from 0 to 1000 eV was used with a pass energy of 100 eV and step size of 1.0 eV. The high-resolution scans were conducted according to the peak being examined with a pass energy of 30 eV and step size of 0.1 eV. All the binding energies were referenced to the C 1*s* hydrocarbon peak at 284.8 eV.

The surface compositions of pristine membrane, cellulose-Br and cellulose-*g*-DADMAC were probed by attenuated total reflection-Fourier transform infrared spectroscopy (ATR-FTIR) using a Perkin-Elmer Spectrum 2000 FTIR spectrometer equipped with a MKII Golden Gate, single reflection ATR System (Specac Ltd., London, UK). The spectra were recorded in the range of 4000–600 cm^{-1} at resolution of 2 cm^{-1} with 64 scans.

The surface morphology of the pristine membrane and cellulose-*g*-DADMAC was observed by a scanning electron microscopy (SEM) instrument (JEOL, JSM-5600 V). The samples were coated with gold for enhancement of conductivity before measurements.

The water contact angle (CA) of the pristine and modified filter membranes was measured using a droplet shape analyzer (KRUSS, DSA 30) by placing a 5 μL water drop on the surface of the membrane. The measurement data were average of 5 different positions.

The Zeta potential of the pristine and modified filter membranes was measured by the streaming current

method with a SurPASS-3 electrokinetic analyzer (Anton-Paar, Austria) and controlled by a Visolab software. The samples (1 cm × 2 cm) were immobilized to the adjustable gap cell. Measurements were carried out using 1 mmol/L of KCl solution, and the pH was adjusted by HCl and NaOH solutions.

To determine the content of Br, the sample was burned with an oxygen bomb and then absorbed by a buffer solution, and the amount of bromine in the liquid is measured using an ion chromatograph (DIONEX, ICS-2000). The cationic density of cellulose-*g*-PDADMAC was obtained using elemental analyzer (Perkin-Elmer, EA 2400 II). The nitrogen content of membranes was determined from the combustion product of NO_X after the sample digestion.

Dye selective removal of cellulose-*g*-PDADMAC

For the selective removal of dye, 20 mL of MO, RB, and MO/RB mixture aqueous solutions with concentration of 50 mg/L for each dye were filtered with the pristine membrane and cellulose-*g*-DADMAC using a custom-made device, respectively. To analyze the decolorization ratio quantitatively, the dye solutions before filtration and filtrates were diluted 10 times, and the concentrations were determined by UV–vis absorption spectroscopy (Agilent, 8453). The decolorization ratio was calculated with the following equation (Alsbaiee et al. 2015):

$$\text{Decolorization ratio} = \frac{C_0 - C_1}{C_0} \times 100\% \quad (2)$$

where C_0 and C_1 are the dye concentrations (mg/L) in the initial and filtrated solution, respectively.

The recyclability of the cellulose-*g*-PDADMAC was measured at room temperature. After each selective removal procedure, the cellulose-*g*-PDADMAC was renewed by immersing into 50 mL of 4 wt% NaCl solution for 20 min, and drying in a vacuum for 2 h. The regenerated cellulose-*g*-PDADMAC was used for the next removal of the dye mixture.

Antibacterial activity of cellulose-*g*-PDADMAC

To evaluate the antibacterial activity of cellulose-*g*-PDADMAC, *E. coli* and *S. aureus* were used as model Gram-negative and Gram-positive pathogenic bacteria, respectively (Roy et al. 2008; Xu et al. 2016). *E. coli* and *S. aureus* were inoculated in Luria–Bertani (LB) growth medium containing peptone (10 g/L), yeast (5 g/L), agar (15 g/L), and NaCl (5 g/L) overnight at 37 °C with constant shaking. The typical colony was taken out by inoculation ring to 50 mL of nutrient broth at 37 °C for 12 h. The concentration of bacteria was $\sim 10^6$ colony forming units (CFU)/mL. The resulting *E. coli* and *S. aureus* suspensions were stored in a sterile medical bottle. The solution was further diluted 100 times to give a working suspension. 5 mL of *E. coli* and *S. aureus* suspensions were added to the bottles containing pristine membrane, and cellulose-*g*-PDADMAC with various graft ratios, respectively. The bottles were incubated at 37 °C for 24 h with 250 rpm. Subsequently, 200 μL of the bacteria culture was taken from each bottle and then spread onto plates of nutrient agar. After incubation at 37 °C for 24 h, the plates were examined. The number of CFU was counted manually. The percent of bacteria reduction was calculated according to the following equation (Kang et al. 2015):

$$\text{Bacteria reduction} = \frac{A - B}{A} \times 100\% \quad (3)$$

where A is the number of bacteria added to sample (CFU/mL) and B is the number of bacteria remaining after incubation (CFU/mL).

Results and discussion

Kinetics of the ATRP of DADMAC initiated by cellulose-Br

The synthesis of cellulose-*g*-PDADMAC is shown in the Fig. 1. BiBB reacts with the accessible hydroxyl groups on the surface of the pristine filter membrane by esterification reaction, binding covalently on the surface of the pristine membrane to form a monolayer of cellulose-Br. The cellulose-Br containing active terminal bromine acted as macroinitiator for the grafting of DADMAC by ATRP (Carlmark and Malmstrom 2002; Wang and Matyjaszewski 1995).

To investigate the kinetics of the ATRP of DADMAC initiated by cellulose-Br, two monomer concentrations, 0.43 mol/L and 0.82 mol/L, were chosen to study the graft ratio as a function of time.

By controlling the concentration of monomer DADMAC and reaction time, the cellulose-*g*-PDADMAC with a series of graft ratios were obtained. Figure 2a shows the relationship of graft ratios of cellulose-*g*-PDADMAC over time. In both conditions, the graft ratio increased with the increase of the reaction time. However, the graft ratio levels off with the progress of the reaction, which is consistent with the reported results (Xiao and Wirth 2002; Xiao et al. 2011). In the process of ATRP, when the amount of initiator and catalyst are controlled quantitatively, the concentration of free radicals should keep constant during the reaction (Nanda and Matyjaszewski 2003). In our study, the amount of Br in cellulose-Br and cellulose-*g*-PDADMAC with graft ratio of 13.3% measured by ion chromatograph was 3.34×10^{-4} mmol/cm^2 and 3.28×10^{-4} mmol/cm^2, respectively. It is obvious the contents of Br decreased after the ATRP reaction. Therefore, the nonlinearity of the relation with reaction time, is attributed to the decrease of monomer concentration, the loss of some Br elements on cellulose-Br, and radical combination termination during the ATRP (Xiao and Wirth 2002; Xiao et al. 2011). Based on the assumption of only radical combination termination for surface-initiated ATRP, the nonlinear time dependence of conversion can be expressed as (Xiao and Wirth 2002; Xiao et al. 2011):

$$[M]_0 - [M] = \frac{[M]_0 k_p [R\cdot]_0 t}{1 + k_t [R\cdot]_0 t} \quad (4)$$

Due to the graft ratio being proportional to $[M]_0 - [M]$, the curves in Fig. 2a fit well with Eq. 4 for both monomer concentrations, as graphed by the solid curves. The propagation rate for the monomer concentration of 0.82 mol/L, i.e. $[M]_0 k_p [R\cdot]_0$, is 1.95-fold (5.193/2.660) faster than that for the monomer concentration of 0.43 mol/L. Considering the ratio of monomer concentration is 0.82/0.43, these two reactions have almost the identical k_p during the polymerization. For the termination rate, the $k_t[R\cdot]_0$ of both monomer concentrations have a similar value (0.165 and 0.158). Consequently, the results and model explained the proportionality of monomer concentration and combination termination.

To further determine the M_n and polydispersity (M_w/M_n) of PDADMAC chains grafted on cellulose-*g*-PDADMAC, the cleaved-off grafts by hydrolysis were determined via GPC. The M_n and M_w/M_n versus monomer conversion of DADMAC for both cases of monomer concentrations, are shown in Fig. 2b. The M_n increased with the increase of monomer conversion. At lower monomer conversion of $< 10\%$, the experimental M_n matched well with theoretical values calculated by $\Delta[M]/[I]_0$. However, at the relatively high conversion, the experimental M_n was higher than the theoretical one due to the combination termination. Meanwhile, with the increase of monomer conversion to 20%, the M_w/M_n of PDADMAC ranged from 1.2 to 1.5, which is < 2.0, indicative of a narrow

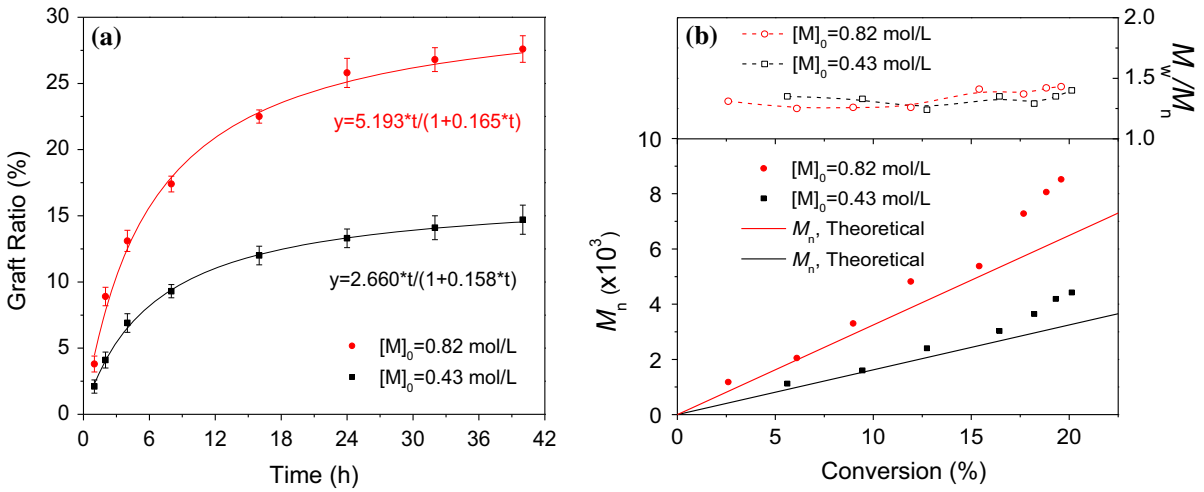

Fig. 2 **a** Graft ratio of cellulose-*g*-PDADMAC versus time, **b** M_n and M_w/M_n versus monomer conversion under conditions of different DADMAC concentrations

polydispersity and controllable polymerization (Xiao and Wirth 2002; Xiao et al. 2011).

ATR-FTIR analysis

Figure 3 shows ATR-FTIR spectra of pristine membrane, cellulose-Br and cellulose-*g*-PDADMAC. The peak at 1055 cm^{-1} in Fig. 3a is related to C–O stretching of the cellulose backbone and is not influenced by reaction (Frisoni et al. 2001), which can be used as the internal standard peak. A new peak at 1739 cm^{-1} in the cellulose-Br (Fig. 3b) is attributed to the carbonyl stretching vibration ($\nu_{C=O}$) (Nyström et al. 2009), indicating that BiBB is immobilized to the surface of filter membrane through ester bonding. In Fig. 3c, two peaks at 1246 cm^{-1} and 1476 cm^{-1} in the cellulose-*g*-PDADMAC are the characteristic bands of $C–N^+$ and the methyl groups of the quaternized ammonium (Zhao et al. 2015), indicating that the surface of filter membrane is successfully grafted DADMAC via ATRP.

XPS analysis

The surface compositions of the pristine membrane, cellulose-Br and cellulose-*g*-PDADMAC were analyzed using XPS, as shown in Fig. 4. The pristine cellulose spectrum (Fig. 4a) only showed O 1*s* and C 1*s* peaks, near 532 eV and 285 eV, respectively. After the immobilization of BiBB on the membrane, a bromine peak (Br 3*d*) appears with a bonding energy at 70.1 eV in Fig. 4c (Wei et al. 2011). The presence of bromine at the surface indicates that the grafting of PDADMAC onto cellulose is a "living" radical polymerization in spite of the loss of Br over the reaction.

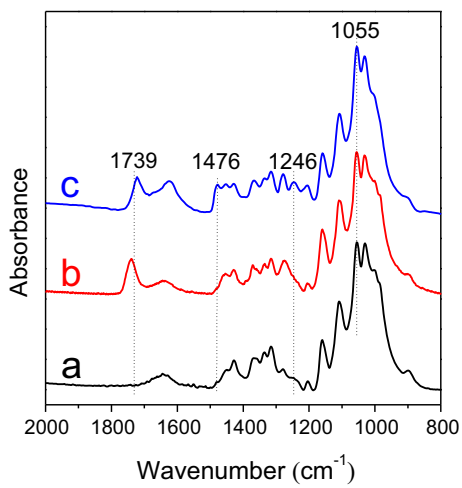

Fig. 3 ATR-FTIR spectra of *a* pristine membrane, *b* cellulose-Br, and *c* cellulose-*g*-PDADMAC with graft ratio of 13.3%

Figure 4b, d show the deconvoluted high resolution C 1*s* spectra in pristine membrane and cellulose-Br. The peaks of pristine membrane at 287.9, 286.6 and 284.8 eV are mainly attributed to the bonds of O–C–O, C–O and C–H/C–C. The intensity of the peak at 286.6 eV is stronger than that at 284.8 and 287.9 eV, showing that the content of C-O species (73.5 at.%) is greater than that of C–H/C–C (7.7 at.%) and O–C–O (18.8 at.%) in the surface of pristine cellulose membrane. Because the BiBB is composed of several C–H/C–C but no C–O species in its molecular chain (Liu et al. 2009), the intensity of C–H/C–C peak of cellulose-Br is higher than that of pristine membrane. The atomic compositions based on the relative peak areas in the survey scans of the investigated samples are summarized in Table 1. As seen in Table 1, the total atomic ratio of O/C decreases from 0.74 to 0.68. The decreased oxygen content in the cellulose-Br suggests that BiBB is successfully introduced on the filter membrane surface.

For the cellulose-*g*-PDADMAC with graft ratio of 13.3% in Fig. 4e, the new peaks at 196.1 eV, 267.1 eV and 402.5 eV are assigned to Cl 2*p*, Cl 2*s* and N 1*s* (Zhong et al. 2012), respectively. The ratio of oxygen to carbon sharply decreased to 0.26, indicating PDADMAC with higher C content was grafted onto the pristine membrane surface. With respect to the narrow scan of C 1*s* peaks in Fig. 4f, the peak at 286.2 eV is mainly attributed to C–N/C–O (Liu et al. 2009). The intensity of C–H/C–C on the cellulose-*g*-PDADMAC surface increases remarkably and is stronger than that of O–C–O indeed. This is because the PDADMAC molecular chain is composed of C–H/C–C and C–N groups but no C–O group. From Table 1, the N/C atomic ratio of cellulose-*g*-PDADMAC is 0.11, which is comparable to the theoretical atomic ratio of 0.125 in PDADMAC. These results indicate that the surface of modified filter membrane is almost covered by the grafted PDADMAC chains.

SEM analysis

The surface morphology of the cellulose filter membranes before and after surface grafting were analyzed

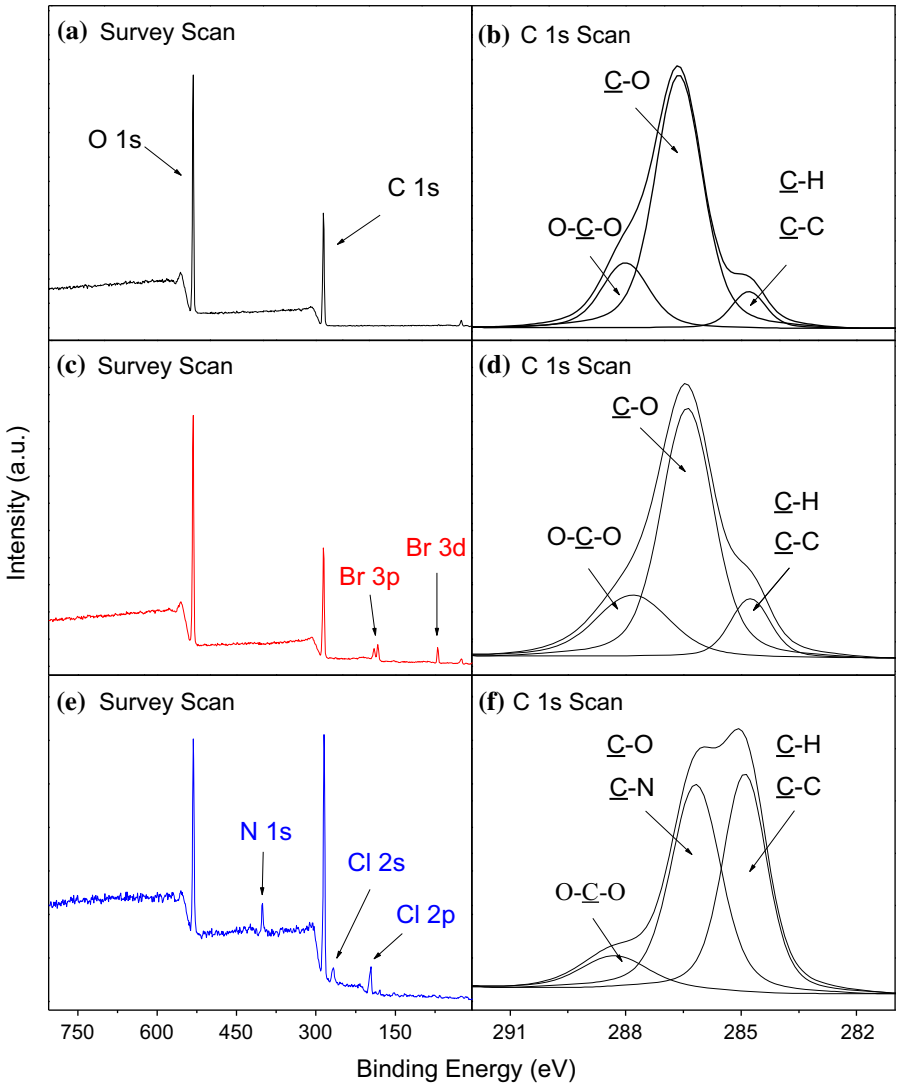

Fig. 4 XPS spectra of **a**, **b** pristine membrane, **c**, **d** cellulose-Br and **e**, **f** cellulose-*g*-PDADMAC with graft ratio of 13.3%

Table 1 Atomic compositions of pristine membrane, cellulose-Br and cellulose-*g*-PDADMAC with graft ratio of 13.3% extracted from XPS

Samples	Element (at.%)					Atomic ratio	
	C	O	Br	N	Cl	O/C	N/C
Pristine membrane	57.6	42.4				0.74	
Cellulose-Br	58.1	39.4	2.5			0.68	
Cellulose-*g*-PDADMAC	68.0	17.9	0.2	7.2	6.7	0.26	0.11

using SEM, as shown in Fig. 5. Porous structure is presented between the cellulose fibers in the pristine membrane (Fig. 5a). Since grafting of PDADMAC occurs mainly on the surface of cellulose fibers (Barsbay et al. 2007; Laopa et al. 2013), no significant changes can be observed in the SEM image of

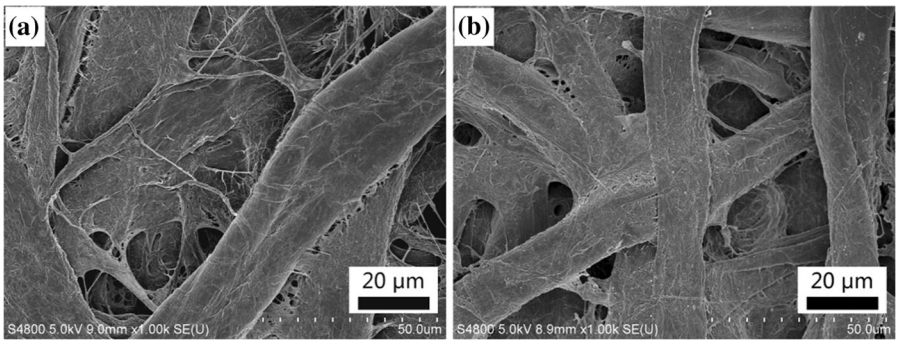

Fig. 5 SEM of **a** pristine membrane and **b** cellulose-*g*-PDADMAC with graft ratio of 13.3%

cellulose-*g*-PDADMAC (Fig. 5b) in comparison to that of the pristine membrane. Due to the electrostatic interaction between the quaternary ammonium group in PDADMAC and the unreacted hydroxyl group on membrane, the PDADMAC has good compatibility with the filter membrane and the surface of cellulose fibers are covered by a thin layer of PDADMAC. Therefore, the surface of the cellulose fiber maintains its porous structure for rapid and facile filtration.

Contact angle analysis

To study the effect of grafted DADMAC on the wettability of the filter membrane, the contact angle measurements of the pristine membrane, cellulose-Br and cellulose-*g*-PDADMAC were conducted, as shown in Fig. 6. The water contact angle of the pristine membrane is $< 10°$ (Fig. 6a), reflecting the natural character of superhydrophilicity because of large amounts of hydroxyl groups in the cellulose. For the macromolecule initiator cellulose-Br, as shown in Fig. 6b, the contact angle significantly increases to $81.7° \pm 2.8°$. The filter membrane surface changes from hydrophilic to hydrophobic significantly. This is because the hydrophobic 2-bromoisobutyryl bromide replaced the hydrophilic hydroxyl groups on cellulose partially, and the introduction of brominated alkyl groups reduced the surface energy of filter membrane.

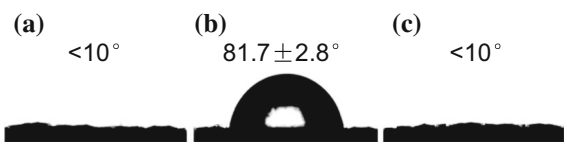

Fig. 6 Micrographs of a water droplet on the surface of **a** pristine membrane, **b** cellulose-Br, and **c** cellulose-*g*-PDADMAC with graft ratio of 13.3%

For cellulose-*g*-PDADMAC in Fig. 6c, the measured contact angle becomes $< 10°$ again, showing the superhydrophilic property. This obvious change is due to the grafted PDADMAC chain on the surface of cellulose-*g*-PDADMAC containing hydrophilic quaternary ammonium groups, which can interact strongly with probing water molecules. This indicates PDADMAC is grafted onto the surface of the filter membrane, which is in agreement with the IR and XPS results.

Selective removal of dye

It is important to remove the dyes selectively from the hazardous dye-based effluents. The selective removal behavior of the cellulose-*g*-PDADMAC was evaluated by filtrating two typical types of dyes, including anionic dye MO and cationic dye RB.

The color of MO solution is orange. After filtration by cellulose-*g*-PDADMAC with graft ratio of 13.3%, the solution color changed from orange to colorless in a short time, as shown in Fig. 7a. The UV–vis spectroscopy was then applied to monitor the removal efficiency of dyes. The absorption peak at 462 nm is the maximum absorption wavelength of MO. After filtration, the 462 nm peak of MO almost disappears. The decolorization ratio calculated from the concentration of dye before and after adsorption is higher than 99.4%. This means the removal efficiency was remarkable and the MO molecules were almost removed from the aqueous conveniently and efficiently by a simple filtration method. However, for the removal of RB (Fig. 7b), no significant color change can be observed before and after filtration. The

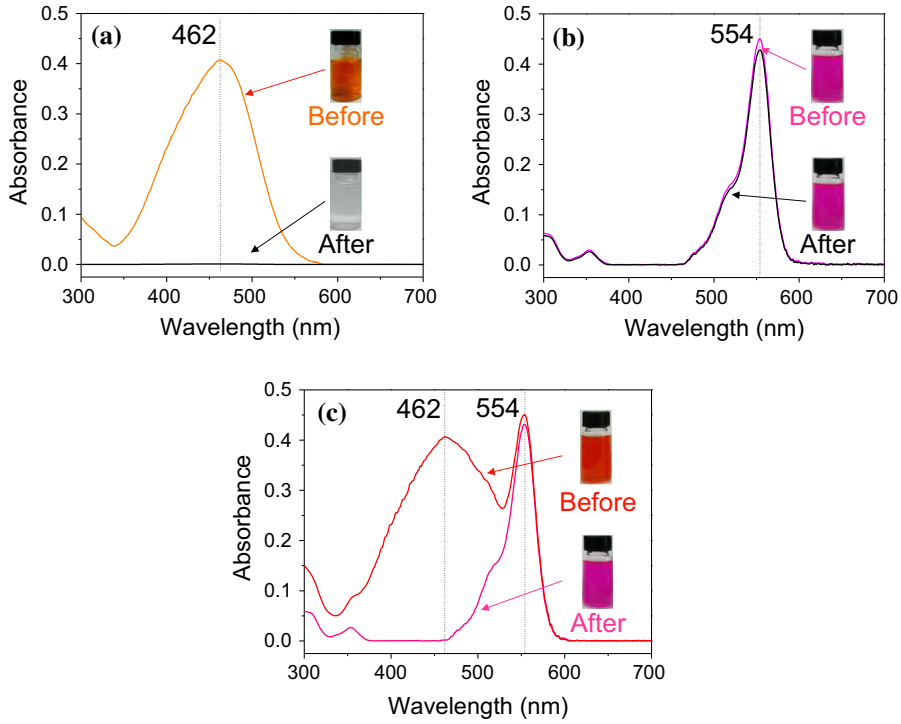

Fig. 7 UV–vis spectra of **a** MO, **b** RB and **c** MO/RB mixture solution before and after filtration by cellulose-*g*-PDADMAC with graft ratio of 13.3%

intensity of the maximum absorption peak of RB at 554 nm decreases slightly after filtration and the calculated decolorization ratio is 4.9%. These results indicate that the dye removal capacity of cellulose-*g*-PDADMAC is effective for the anionic dye MO, but poor for cationic dye RB.

To further measure the selective removal of dyes, the mixture solution of MO and RB was tested. The mixture solution passed through the filter membrane under gravity. Before separation as shown in Fig. 7c, both the strong absorption peak of MO at 462 nm and the maximum absorption of RB at 554 nm appear in the UV–vis spectra of mixed solution. For the pristine filter membrane, the color of filtrate barely changes after filtration (see Video 1 in Supplementary Information) and the center of pristine membrane is pink. The calculated decolorization ratio of MO and RB was 0.9% and 8.4%. This indicates that both MO and RB pass through the membrane simultaneously and no obvious selective separation behavior is displayed.

With respect to cellulose-*g*-PDADMAC membrane during the filtration (see Video 2 in Supplementary Information), the color of solution changes from red to pink, showing the color of RB. The center of cellulose-*g*-PDADMAC turns to deep orange, indicating that large amounts of MO molecules are absorbed on the cellulose-*g*-PDADMAC. In the UV–vis spectra, the characteristic absorption peak of MO at 462 nm in the filtrate is not visible, while the maximum wavelength absorption peak of RB at 554 nm remains strong. The decolorization ratio of MO is 99.1% and that of RB is 4.1%, indicating the remarkable selective separation for the dye mixture. Furthermore, the permeation flux (679 L/m^2/h) of cellulose-*g*-PDADMAC membrane is comparable to that of the pristine membrane driven solely by gravity. It should be noted that permeation flux will increase under external driving pressures. A high decolorization ratio of more than 98.4% for MO was maintained as the permeation flux approached 1455 L/m^2/h. To further evaluate the removal capacity, the cellulose-*g*-PDADMAC with graft ratio of 13.3% was examined. The calculated cationic density of filter membrane is about 0.0067 mmol/cm^2 by elemental analysis. At the permeation flux of 679 L/m^2/h, 1.22 mg of MO can be captured by 1 cm^2 of cellulose-*g*-PDADMAC. This means 1 mol of cationic quaternized ammonium can adsorb 0.56 mol of anionic MO, which is higher than the reported materials such as MOF membranes and supramolecular gels (Cheng et al. 2015; Park and Oh 2017).

Meanwhile, the maximum adsorption (Q_{max}) of cellulose-*g*-PDADMAC for MO is examined, which is 182.6 mg per gram of cellulose-*g*-PDADMAC. Therefore, our cellulose-*g*-PDADMAC membranes display selective removal for anionic MO via rapid and facile filtration.

To examine the effect of graft ratio on decolorization ratio of MO and RB mixture, the cellulose-*g*-PDADMAC with different graft ratios was used for the dye removal. With the increase of graft ratio, the decolorization ratio of MO increases dramatically, as shown in Fig. 8. When the graft ratio is 2.4%, the decolorization ratio progressively attains up to 91.5%. As the graft ratio increases, the decolorization ratio reaches a stable value gradually. When the graft ratio is increased to 25.8%, the decolorization ratio is as high as 99.3%. On the contrary, the decolorization ratio of RB decreases with the increase of graft ratio gradually and the lowest value is about 3.7%, showing poor efficiency on the removal of RB.

To evaluate the surface charge property of the cationic polymer modified cellulose membranes for the selectivity of MO adsorption, the Zeta potential of cellulose-*g*-DADMAC membrane was measured. At the pH value of 6.9, the Zeta potential of unmodified filter membrane is -19.3 ± 1.2 mV, showing that the pristine cellulose surface is negatively charged due to the large amounts of hydroxyl groups. After grafting the quaternary ammonium groups, the Zeta potential of cellulose-*g*-PDADMAC changes to 17.7 ± 1.0 mV and the surface becomes positively charged. This endows cellulose-*g*-PDADMAC to capture anionic organic dyes selectively.

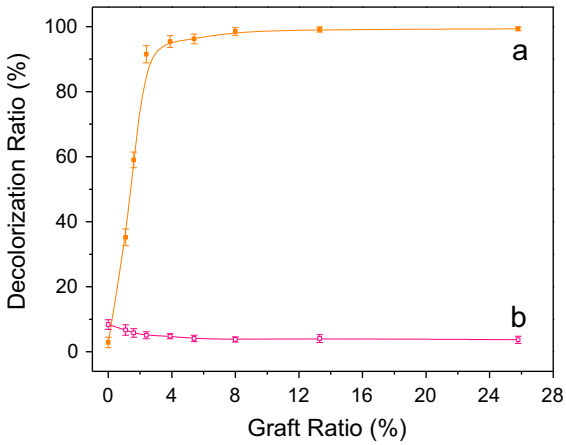

Fig. 8 Effect of cellulose-*g*-PDADMAC with different graft ratio on decolorization ratio of *a* MO and *b* RB in mixture

The schematic of selective removal of dyes by cellulose-*g*-PDADMAC is shown in Fig. 9. The selective removal of mixed dyes can be demonstrated by the electrostatic interaction between the PDADMAC chains and the dye molecules (Xie et al. 2014). The surface of cellulose-*g*-PDADMAC contains cationic quaternary ammonium PDADMAC with high density of positive charges. MO is an anionic dye within the sulfonic acid group. When the dye solution goes through the cellulose-*g*-PDADMAC membrane, the MO molecules are adsorbed and held in its surface due to the electrostatic attractive interaction between quaternary ammonium groups and the sulfonic groups. However, as a cationic dye with cationic quaternary ammonium, RB passes through the modified membrane due to electrostatic repulsion of PDADMAC to RB. Thus the electrostatic interactions dominate the selective removal performance of cellulose-*g*-PDADMAC.

In addition, the effect of pore size of membranes on the selective removal behavior is considered. The nominal pore size of cellulose filter membrane we used is about 1–3 μm, which is much larger than the size of dye molecules (0.28–1.54 nm) (Ifuku and Kadla 2008). Therefore, the separation of dyes cannot account for the physical interception which depends on the pore size of membrane.

Recyclability

The recyclability of the cellulose-*g*-PDADMAC for selective removal of dye mixture is significant for environmental protection. To investigate the recyclability, cellulose-*g*-PDADMAC was renewed by immersing into NaCl solution before each separation cycle. As shown in Fig. 10, the decolorization ratio of MO remains higher than 95% and the decolorization ratio of RB is lower than 6% after 6 cycles. As a result, cellulose-*g*-PDADMAC is stable and recyclable for selective removal of anionic dye, which is important for its practical application.

Antimicrobial effects of cellulose-g-PDADMAC

The highly positive charges impart cellulose-*g*-PDADMAC with antibacterial properties against negatively charged bacteria, via electrostatic

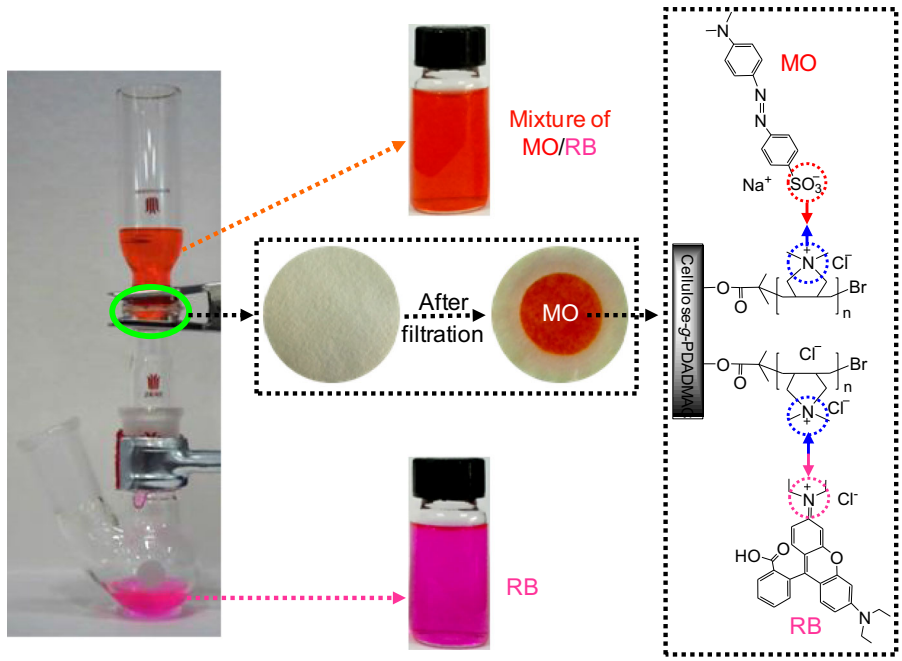

Fig. 9 The schematic of selective removal of dyes by cellulose-*g*-PDADMAC

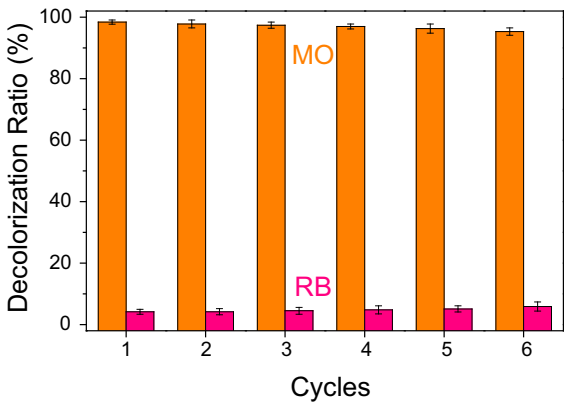

Fig. 10 Recyclability of cellulose-*g*-PDADMAC

interactions (Fu et al. 2017). To evaluate the antimicrobial effects against various microorganisms, two representative microorganisms, *S. aureus* and *E. coli* were used for determining the antibacterial activity of cellulose-*g*-PDADMAC, as shown in Fig. 11. The pristine membrane and cellulose-*g*-PDADMAC with different graft ratios were examined by immersion into the *E. coli* and *S. aureus* suspensions, as shown in Fig. 11A. The turbidity of suspensions is related to the number of bacteria. The higher turbidity reflects a

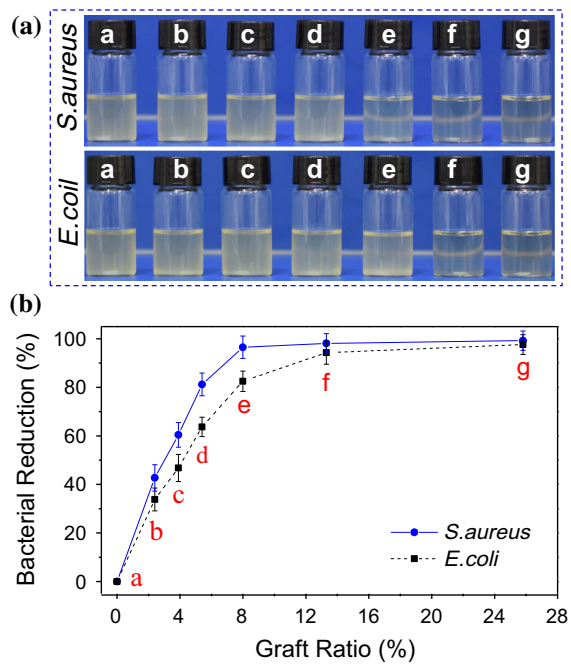

Fig. 11 **A** Images for antibacterial activity of (*a*) pristine filter membrane and cellulose-*g*-PDADMAC with graft ratio of (*b*) 2.4%, (*c*) 3.9%, (*d*) 5.4%, (*e*) 8.0%, (*f*) 13.3%, and (*g*) 25.8% against *S. aureus* and *E. coli*, **B** relationship of graft ratio on bacterial reduction

lesser antibacterial activity. In the culture bottle with the pristine membrane (Fig. 11Aa), both bottles present high turbidity and vigorous bacteria growth, suggesting that unmodified cellulose has no antibacterial activity. By contrast, the bottles with cellulose-*g*-PDADMAC having various graft ratios show different turbidity and antibacterial activity. When the graft ratio is 8.0%, the *S. aureus* suspension turns to relatively clear, while the *E. coli* suspension changes to relatively clear when graft ratio was 13.3%.

To further assess the effect of graft ratio on antibacterial efficiency, the bacterial reduction of the cellulose-*g*-PDADMAC with various graft ratios is shown in Fig. 11B. For these two bacteria, a similar trend is observed. With the increase of graft ratio, the bacterial reduction increases significantly. When the graft ratio reaches 13.3%, the bacterial reduction of *S. aureus* is about 98.1%, and that of *E. coli* is about 92.3%, showing a strong inhibition effect. Meanwhile, the cellulose-*g*-PDADMAC exhibit higher inhibition to *S. aureus* than *E. coli*, which is similar to the reported results (Song et al. 2010). This is because the porous structure of the *S. aureus* cell wall makes the foreign molecules enter the cell easily, while the thin film of the cell wall of *E. coli* is a potential barrier against foreign molecules (Sun et al. 2006). The effective antimicrobial activities of cellulose-*g*-PDADMAC enhanced the stability of filter membrane for application in textile industry.

Conclusions

In this paper, cellulose-*g*-PDADMAC was fabricated via surface-initiated ATRP concept. GPC, XPS, and FTIR showed that PDADMAC was grafted onto the filter membrane surface via a controllable living polymerization. Due to electrostatic interaction between the quaternary ammonium group on cellulose-*g*-PDADMAC and the sulfonic group on MO, the modified filter membrane exhibited rapid selective removal of anionic MO from anionic dye-containing wastewater with good recyclability. The cellulose-*g*-PDADMAC with graft ratio of 13.3% has a bacterial reduction of 98.1% against *S. aureus* and 92.3% against *E. coli*, showing a strong inhibition effect. The selective removal of anionic dye and good antimicrobial activity offer cellulose-*g*-PDADMAC a great potential for treatment of dye wastewater in practice. In the near future, cellulose will be further modified to obtain multi-functional cellulose-based materials for the application in adhesive, self-healing hydrogel, and wound dressing.

Supplementary material

Video of MO/RB mixture solution filtrated by pristine filter membrane and cellulose-*g*-PDADMAC.

Acknowledgments This work was supported by the National Natural Science Foundation of China (31470598, 21774021), the Award Program for Minjiang Scholar Professorship, and International Science and Technology Cooperation and Exchange Project of Fujian Agriculture and Forestry University (KXb16002A).

References

Alsbaiee A, Smith BJ, Xiao L, Ling Y, Helbling DE, Dichtel WR (2015) Rapid removal of organic micropollutants from water by a porous β-cyclodextrin polymer. Nature 529:190

Barsbay M, Güven O, Stenzel MH, Davis TP, Barner-Kowollik C, Barner L (2007) Verification of controlled grafting of styrene from cellulose via radiation-induced RAFT polymerization. Macromolecules 40:7140–7147

Carlmark A, Malmstrom E (2002) Atom transfer radical polymerization from cellulose fibers at ambient temperature. J Am Chem Soc 124:900–901

Chen Z, Zhang J, Xiao P, Tian W, Zhang J (2018) Novel thermoplastic cellulose esters containing bulky moieties and soft segments. ACS Sustain Chem Eng 6:4931–4939

Cheng N, Hu QZ, Guo YX, Wang Y, Yu L (2015) Efficient and selective removal of dyes using imidazolium-based supramolecular gels. ACS Appl Mater Interfaces 7:10258–10265

Crini G (2006) Non-conventional low-cost adsorbents for dye removal: a review. Biores Technol 97:1061–1085

Daraei P, Ghaemi N, Sadeghi Ghari H (2017) An ultra-antifouling polyethersulfone membrane embedded with cellulose nanocrystals for improved dye and salt removal from water. Cellulose 24:915–929

Dragan ES, Dinu MV (2018) Spectacular selectivity in the capture of methyl orange by composite anion exchangers with the organic part hosted by DAISOGEL microspheres. ACS Appl Mater Interfaces 10:20499–20511

Edgar KJ (2007) Cellulose esters in drug delivery. Cellulose 14:49–64

Frisoni G, Baiardo M, Scandola M, Lednická D, Cnockaert MC, Mergaert J, Swings J (2001) Natural cellulose fibers: heterogeneous acetylation kinetics and biodegradation behavior. Biomacromolecules 2:476–482

Fu G, Su Z, Jiang X, Yin J (2014) Photo-crosslinked nanofibers of poly(ether amine) (PEA) for the ultrafast separation of

dyes through molecular filtration. Polym Chem 5:2027–2034

Fu Y, Jiang J, Zhang Q, Zhan X, Chen F (2017) Robust liquid-repellent coatings based on polymer nanoparticles with excellent self-cleaning and antibacterial performances. J Mater Chem A 5:275–284

Gopakumar DA, Pasquini D, Henrique MA, de Morais LC, Grohens Y, Thomas S (2017) Meldrum's acid modified cellulose nanofiber-based polyvinylidene fluoride microfiltration membrane for dye water treatment and nanoparticle removal. ACS Sustain Chem Eng 5:2026–2033

Gupta VK, Suhas (2009) Application of low-cost adsorbents for dye removal—a review. J Environ Manag 90:2313–2342

Habibi Y (2014) Key advances in the chemical modification of nanocelluloses. Chem Soc Rev 43:1519–1542

Hokkanen S, Bhatnagar A, Sillanpää M (2016) A review on modification methods to cellulose-based adsorbents to improve adsorption capacity. Water Res 91:156–173

Ifuku S, Kadla JF (2008) Preparation of a thermosensitive highly regioselective cellulose/*N*-isopropylacrylamide copolymer through atom transfer radical polymerization. Biomacromolecules 9:3308–3313

Kang J, Han J, Gao Y, Gao T, Lan S, Xiao L, Zhang Y, Gao G, Chokto H, Dong A (2015) Unexpected enhancement in antibacterial activity of N-halamine polymers from spheres to fibers. ACS Appl Mater Interfaces 7:17516–17526

Laopa PS, Vilaivan T, Hoven VP (2013) Positively charged polymer brush-functionalized filter paper for DNA sequence determination following Dot blot hybridization employing a pyrrolidinyl peptide nucleic acid probe. Analyst 138:269–277

Lin QW, Gao MF, Chang JL, Ma HZ (2016a) Adsorption properties of crosslinking carboxymethyl cellulose grafting dimethyldiallylammonium chloride for cationic and anionic dyes. Carbohydr Polym 151:283–294

Lin X, Ma W, Wu H, Cao S, Huang L, Chen L, Takahara A (2016b) Superhydrophobic magnetic poly(DOPAm-*co*-PFOEA)/Fe_3O_4/cellulose microspheres for stable liquid marbles. Chem Commun 52:1895–1898

Liu P-S, Chen Q, Liu X, Yuan B, Wu S-S, Shen J, Lin S-C (2009) Grafting of Zwitterion from cellulose membranes via ATRP for improving blood compatibility. Biomacromolecules 10:2809–2816

Mathieu-Denoncourt J, Martyniuk CJ, de Solla SR, Balakrishnan VK, Langlois VS (2014) Sediment contaminated with the azo dye disperse Yellow 7 alters cellular stress- and androgen-related transcription in *Silurana tropicalis* larvae. Environ Sci Technol 48:2952–2961

Min MH, Shen LD, Hong GS, Zhu MF, Zhang Y, Wang XF, Chen YM, Hsiao BS (2012) Micro-nano structure poly(-ether sulfones)/poly(ethyleneimine) nanofibrous affinity membranes for adsorption of anionic dyes and heavy metal ions in aqueous solution. Chem Eng J 197:88–100

Mittal A, Malviya A, Kaur D, Mittal J, Kurup L (2007) Studies on the adsorption kinetics and isotherms for the removal and recovery of Methyl Orange from wastewaters using waste materials. J Hazard Mater 148:229–240

Nanda AK, Matyjaszewski K (2003) Effect of PMDETA/Cu(I) ratio, monomer, solvent, counterion, ligand, and alkyl bromide on the activation rate constants in atom transfer radical polymerization. Macromolecules 36:1487–1493

Nyström D, Lindqvist J, Östmark E, Antoni P, Carlmark A, Hult A, Malmström E (2009) Superhydrophobic and self-cleaning bio-fiber surfaces via ATRP and subsequent postfunctionalization. ACS Appl Mater Interfaces 1:816–823

Park J, Oh M (2017) Construction of flexible metal-organic framework (MOF) papers through MOF growth on filter paper and their selective dye capture. Nanoscale 9:12850–12854

Pendergast MM, Hoek EMV (2011) A review of water treatment membrane nanotechnologies. Energy Environ Sci 4:1946–1971

Qiao H, Zhou Y, Yu F, Wang E, Min Y, Huang Q, Pang L, Ma T (2015) Effective removal of cationic dyes using carboxylate-functionalized cellulose nanocrystals. Chemosphere 141:297–303

Ran J, Wu L, Zhang Z, Xu T (2014) Atom transfer radical polymerization (ATRP): a versatile and forceful tool for functional membranes. Prog Polym Sci 39:124–144

Roy D, Knapp JS, Guthrie JT, Perrier S (2008) Antibacterial cellulose fiber via RAFT surface graft polymerization. Biomacromolecules 9:91–99

Song YB, Zhang J, Gan WP, Zhou JP, Zhang LN (2010) Flocculation properties and antimicrobial activities of quaternized celluloses synthesized in NaOH/urea aqueous solution. Ind Eng Chem Res 49:1242–1246

Sui XF, Yuan JY, Zhou M, Zhang J, Yang HJ, Yuan WZ, Wei Y, Pan CY (2008) Synthesis of cellulose-graft-poly(*N*, *N*-dimethylamino-2-ethyl methacrylate) copolymers via homogeneous ATRP and their aggregates in aqueous media. Biomacromolecules 9:2615–2620

Sun LP, Du YM, Fan LH, Chen X, Yang JH (2006) Preparation, characterization and antimicrobial activity of quaternized carboxymethyl chitosan and application as pulp-cap. Polymer 47:1796–1804

Tang Z, Li W, Lin X, Xiao H, Miao Q, Huang L, Chen L, Wu H (2017) TEMPO-oxidized cellulose with high degree of oxidation. Polymers 9:421

Tian H, He J (2016) Cellulose as a scaffold for self-assembly: from basic research to real applications. Langmuir 32:12269–12282

Wang J-S, Matyjaszewski K (1995) Controlled/"living" radical polymerization. Atom transfer radical polymerization in the presence of transition-metal complexes. J Am Chem Soc 117:5614–5615

Wang S, Lu A, Zhang L (2016) Recent advances in regenerated cellulose materials. Prog Polym Sci 53:169–206

Wei YT, Zheng YM, Chen JP (2011) Functionalization of regenerated cellulose membrane via surface initiated atom transfer radical polymerization for boron removal from aqueous solution. Langmuir 27:6018–6025

Wen Y, Wei B, Cheng D, An X, Ni Y (2017) Stability enhancement of nanofibrillated cellulose in electrolytes through grafting of 2-acrylamido-2-methylpropane sulfonic acid. Cellulose 24:731–738

Wu H, Higaki Y, Takahara A (2018) Molecular self-assembly of one-dimensional polymer nanostructures in nanopores of anodic alumina oxide templates. Prog Polym Sci 77:95–117

Würfel H, Kayser M, Heinze T (2018) Efficient and catalyst-free synthesis of cellulose acetoacetates. Cellulose 25:4919–4928

Xiao D, Wirth MJ (2002) Kinetics of surface-initiated atom transfer radical polymerization of acrylamide on silica. Macromolecules 35:2919–2925

Xiao M, Li S, Chanklin W, Zheng A, Xiao H (2011) Surface-initiated atom transfer radical polymerization of butyl acrylate on cellulose microfibrils. Carbohydr Polym 83:512–519

Xie Y, Yan B, Xu H, Chen J, Liu Q, Deng Y, Zeng H (2014) Highly regenerable mussel-inspired Fe_3O_4@polydopamine-Ag core–shell microspheres as catalyst and adsorbent for methylene blue removal. ACS Appl Mater Interfaces 6:8845–8852

Xu WZ, Yang L, Charpentier PA (2016) Preparation of antibacterial softwood via chemical attachment of quaternary ammonium compounds using supercritical CO_2. ACS Sustain Chem Eng 4:1551–1561

Yan JJ, Huang YP, Miao YE, Tjiu WW, Liu TX (2015) Polydopamine-coated electrospun poly(vinyl alcohol)/poly(-acrylic acid) membranes as efficient dye adsorbent with good recyclability. J Hazard Mater 283:730–739

Yang L, Wang Z, Zhang J (2017a) Zeolite imidazolate framework hybrid nanofiltration (NF) membranes with enhanced permselectivity for dye removal. J Membr Sci 532:76–86

Yang XF, Liu GQ, Peng L, Guo JH, Tao L, Yuan JY, Chang CY, Wei Y, Zhang LN (2017b) Highly efficient self-healable and dual responsive cellulose-based hydrogels for controlled release and 3D cell culture. Adv Func Mater 27:1703134

Yao L, Zhang LZ, Wang R, Chou SR, Dong ZL (2016) A new integrated approach for dye removal from wastewater by polyoxometalates functionalized membranes. J Hazard Mater 301:462–470

Zhang H, Luan Q, Tang H, Huang F, Zheng M, Deng Q, Xiang X, Yang C, Shi J, Zheng C, Zhou Q (2017) Removal of methyl orange from aqueous solutions by adsorption on cellulose hydrogel assisted with Fe_2O_3 nanoparticles. Cellulose 24:903–914

Zhao X, Ma HR, Ma JZ, Gao DG, Xu J, Hua L (2015) Aerobic biodegradation of polydiallyldi-methylammonium chloride-acrylic-acrylamide-hydroxyethyl acrylate/ZnO nanocomposite in an activated sludge system. RSC Adv 5:21277–21284

Zhong PS, Widjojo N, Chung TS, Weber M, Maletzko C (2012) Positively charged nanofiltration (NF) membranes via UV grafting on sulfonated polyphenylenesulfone (sPPSU) for effective removal of textile dyes from wastewater. J Membr Sci 417:52–60

Zhou X, Lin X, White KL, Lin S, Wu H, Cao S, Huang L, Chen L (2016) Effect of the degree of substitution on the hydrophobicity of acetylated cellulose for production of liquid marbles. Cellulose 23:811–821

Zoppe JO, Xu X, Känel C, Orsolini P, Siqueira G, Tingaut P, Zimmermann T, Klok H-A (2016) Effect of surface charge on surface-initiated atom transfer radical polymerization from cellulose nanocrystals in aqueous media. Biomacromolecules 17:1404–1413